JASA ARTICLE

Wideband acoustic immittance: Suitable quantities for assessing middle-ear status

Kren Monrad Nørgaard,[1,2,a] Jingxin Jessica Feng,[3] and Susan E. Voss[3]
[1]*Interacoustics Research Unit, 2800 Kongens Lyngby, Denmark*
[2]*Interacoustics A/S, 5500 Middelfart, Denmark*
[3]*Picker Engineering Program, Smith College, Northampton, Massachusetts 01063, USA*

ABSTRACT:
This paper investigates the physical significance of ear-canal wave quantities—such as absorbance—that are commonly measured in wideband-acoustic-immittance tests and evaluates whether these quantities uniquely characterize middle-ear function. This is explored using simulations of lumped-element and transmission-line ear canals, along with measurements in three-dimensional-printed uniform and anatomical ear canals of varying geometry, terminated by the same middle-ear simulator. The results demonstrate the following points: (1) Wave quantities computed using estimated or geometrical cross-sectional areas do not uniquely characterize the middle ear because they describe the wave interaction between ear canal and middle ear and are therefore confounded by variations in ear-canal geometry. (2) At low frequencies, the reflection of sound waves in the ear canal plays a negligible role in the middle-ear transduction mechanism because of the long sound wavelength relative to ear-canal length, and wave quantities therefore do not provide a meaningful physical characterization of middle-ear function. (3) Wave quantities computed using an invariant cross-sectional area are likely most appropriate for clinical diagnostics, as they reduce the influence of ear-canal geometry up to approximately 3 kHz. However, this simplification means that wave quantities no longer characterize the reflection of sound waves in the ear canal at any frequency. © *2026 Acoustical Society of America*.
https://doi.org/10.1121/10.0043164
(Received 9 January 2026; revised 3 March 2026; accepted 6 March 2026; published online 25 March 2026)
[Editor: Christopher Shera] Pages: 2857–2874

I. INTRODUCTION

The acoustic immittance (admittance and impedance) of the auditory system has long been a subject of interest to researchers and clinicians both to understand the mechanics of and to diagnose pathologies in the human middle ear. Conventional tympanometry is a crucial clinical tool for diagnosing common middle-ear disorders that involves measuring the ear-canal admittance at a single probe-tone frequency, usually 226 Hz, while varying the ear-canal air pressure at a constant rate and estimating the middle-ear admittance at the peak of the tympanogram. The middle-ear admittance uniquely characterizes the acoustic mobility of the middle ear across the surface of the tympanic membrane and is typically estimated from measurements in the ear canal, away from the tympanic membrane, by removing the effects of the residual ear-canal space from the ear-canal admittance. At low frequencies, the lumped-element admittance of this ear-canal space is approximated as the ear-canal admittance at the tail of the tympanogram—i.e., at the first air-pressure extreme, assuming rigidity of the tympanic membrane at this pressure—and simply subtracted from the ear-canal admittance. However, toward higher frequencies, ear-canal standing waves start to form, affecting the ear-canal admittance, and an ear-canal model taking into account at least one-dimensional wave propagation is required to estimate the middle-ear admittance.

Ear-canal wave quantities characterize proportions of sound waves in the ear canal reflected or absorbed by the middle ear and were first measured by Stinson *et al.* (1982),[1] who estimated the ear-canal energy reflection coefficient (energy reflectance) from the standing-wave ratio. The length of the ear canal naturally limits the lower frequency at which this technique is applicable. Hudde (1983) noted the small dependence of the ear-canal pressure-reflectance magnitude on measurement location and proposed this quantity as a means for characterizing the middle ear at higher frequencies because of the inherent transmission-line effects in the ear canal in this frequency region. Enabled by the advent of digital data-acquisition systems and the ear-probe calibration procedure described by Allen (1986), complex ear-canal pressure reflectance—calculated from the ear-canal impedance and characteristic impedance—has been routinely measured in human ears across most of the audio bandwidth using ear probes over the past 40 years. The ear-canal pressure-reflectance magnitude is closely related to alternative wave quantities, the scalar energy reflectance and absorbance, which all characterize the same physical phenomenon, and energy absorbance is routinely used for middle-ear diagnostics in the clinic. Under the assumption of a uniform ear canal, these wave quantities characterize sound-wave reflections by the middle ear that,

[a]Email: krng@interacoustics.com

unlike ear-canal admittance, are insensitive to ear-probe placement. Ear-canal wave quantities have shown potential in diagnosing and differentiating between conductive hearing disorders beyond what is possible with conventional tympanometry (e.g., early work by Piskorski *et al.*, 1999; Keefe *et al.*, 2000; Feeney *et al.*, 2003; Keefe and Simmons, 2003) and can be measured without pressurizing the ear canal. These wave quantities, along with ear-canal impedance and admittance, measured across a wide range of frequencies, are collectively referred to as wideband acoustic immittance (WAI; Feeney *et al.*, 2013). For clarity, we will refer to WAI here only as the overarching objectives of improving clinical diagnosis of the middle ear and physically characterizing the middle ear across a wide range of frequencies and refrain from using this term to refer to wave quantities, which are inherently not immittance quantities. The measurement of ear-canal wave quantities is currently offered by several clinical instruments, including the HearID and OtoStat (Mimosa Acoustics, Inc., Champaign, Illinois, USA), the Titan (Interacoustics A/S, Middelfart, Denmark), and the TympStar Pro (Grason-Stadler, Inc., Eden Prairie, Minnesota, USA). Nonetheless, difficulty in the interpretation of wave quantities is often cited as an obstacle for clinical adoption (Al-Salim *et al.*, 2024).

The objective of this paper is to discuss and iterate the physical significance of ear-canal wave quantities and investigate whether these quantities are the most suitable for characterizing the middle ear, both physically and clinically. This will be achieved using simple lumped-element and transmission-line simulations, as well as measurements in three-dimensional (3D)-printed uniform and anatomical ear canals, terminated by the same middle-ear simulator.

II. BACKGROUND

In most research involving the measurement of ear-canal wave quantities using a conventional ear probe, the ear-canal impedance Z_{ec} is calculated from the ear-canal pressure P_{ec} measured by the ear-probe microphone and the ear-probe acoustic Thévenin-equivalent parameters, the source pressure P_s and source impedance Z_s, obtained in a preceding calibration procedure (Allen, 1986; Keefe *et al.*, 1992; Voss and Allen, 1994),

$$Z_{ec} = Z_s \frac{P_{ec}}{P_s - P_{ec}}. \tag{1}$$

Because the WAI literature typically deals with impedance Z rather than admittance Y, we will maintain this notion throughout Secs. II and III in this paper, but results will be reported in terms of admittance,

$$Y = \frac{1}{Z}, \tag{2}$$

because it is conventionally and intuitively used for assessing middle-ear status. Some publications have utilized mathematically equivalent methods for characterizing the ear probe based on acoustic Norton-equivalent (Huang *et al.*, 2000) or reflectance (Keefe, 1997; Keefe and Simmons, 2003) parameters. The ear-canal pressure reflectance R_{ec} is defined as the complex ratio of reverse-propagating P_- to forward-propagating P_+ pressure waves in the ear canal. Assuming that the ear canal is a lossless uniform transmission line with characteristic impedance $Z_0 = \rho c/S_{ec}$, with the air density ρ, the speed of sound c, and the cross-sectional area S_{ec},

$$R_{ec} = \frac{P_-}{P_+} = \frac{Z_{ec}/Z_0 - 1}{Z_{ec}/Z_0 + 1}. \tag{3}$$

Here, Z_{ec}/Z_0 is often referred to as the normalized impedance, the mathematical importance of which will become evident later (Sec. V C). Because measuring the geometrical ear-canal cross-sectional area S_{ec} is impractical in clinical scenarios, previous studies have assumed an invariant area (Voss and Allen, 1994) or acoustically estimated the ear-canal characteristic impedance $\hat{Z}_0$, implicitly estimating the area $\hat{S}_{ec}$ (e.g., Keefe *et al.*, 1992; Rasetshwane and Neely, 2011; Nørgaard *et al.*, 2017a, 2019c). The scalar ear-canal energy reflectance $|R_{ec}|^2$ is occasionally considered, but the scalar ear-canal energy absorbance A_{ec} is conventionally used for the purpose of clinical diagnosis, mainly because it is analogous to the admittance in characterizing how well sound is transmitted by the middle ear, and is usually derived from $|R_{ec}|^2$ by conservation of energy,

$$A_{ec} = \frac{|P_+|^2 - |P_-|^2}{|P_+|^2} = 1 - |R_{ec}|^2. \tag{4}$$

The ear-canal pressure absorbance $[(P_+ - P_-)/P_+ = 1 - R_{ec}]$ has not previously been reported because its magnitude depends on the ear-canal length, thus lacking a key benefit of the remaining ear-canal wave quantities. This is because, unlike energy, pressure magnitude is not conserved across a boundary, so the calculation of middle-ear pressure-absorbance magnitude requires propagation of individual wave components to the tympanic membrane. For this reason, absorbance without further specification usually refers to energy absorbance. Temporal characteristics of the ear-canal reflectance, such as the phase and group delays,

$$\tau_\phi = -\frac{\angle R_{ec}}{\omega} \text{ and } \tau_g = -\frac{\mathrm{d}\angle R_{ec}}{\mathrm{d}\omega}, \tag{5}$$

respectively, with the unwrapping phase operator $\angle$ and the angular frequency ω, have primarily been used to estimate ear-canal length (e.g., Keefe *et al.*, 2015; Nørgaard *et al.*, 2020).

The fundamental nature of the various relevant ear-canal wave quantities—the pressure reflectance, energy reflectance, and energy absorbance—representing the proportion of sound pressure or energy reflected or absorbed by

https://doi.org/10.1121/10.0043164

the middle ear has been emphasized by the majority of publications dealing with the subject matter. Many studies have also emphasized the insensitivity of wave-quantity magnitudes on measurement location, a feature that is understandably highlighted as a metrological advantage over immittance quantities. Surprisingly few articles have commented in more detail on additional properties of wave quantities: Keefe *et al.* (1992) noted that the ear-canal impedance, unlike reflectance, encodes information about the ear-canal characteristic impedance, and Voss and Allen (1994) highlighted certain advantageous signal-processing properties of reflectance over immittance. To our knowledge, only a single study has commented on and questioned the suitability of ear-canal wave quantities in actually characterizing the properties of the middle ear; Huang *et al.* (2000) noted the inability of the reflectance in uniquely characterizing the mechanics of the middle ear, however, exemplified it rather vaguely as an inability in distinguishing mass-like and compliance-like responses. In addition to the few comments made in these articles, the broader transition in the literature from characterizing the middle ear by its mechanical mobility using admittance to its ability to absorb sound-wave energy using absorbance has been uncritical, and the fundamental differences between characterizing the middle ear using immittance and wave quantities remain poorly articulated.

This paper offers a basis for the critical evaluation and conversation needed regarding the characterization of middle-ear status using wave quantities and their interpretation and is motivated by the following observations:

(1) *Ear-canal cross-sectional area and non-uniformity:* The ear canal is inherently non-uniform, thus violating the assumption of plane waves underlying wave quantities. This non-uniformity is known to introduce intra-subject variability because measurements depend on location-specific partial reflections from the ear-canal walls. However, as neither the measurement location nor the local cross-sectional area is known prior to a measurement, this area must be approximated or estimated to calculate wave quantities. In uniform waveguides, the cross-sectional area can be accurately estimated (Nørgaard *et al.*, 2019a), and in ear canals, the estimated cross-sectional area using the method of Nørgaard *et al.* (2019c) yields more accurate reflectance measurements in adult ears (Nørgaard *et al.*, 2020). However, the physical significance of such estimated cross-sectional areas in varying anatomical ear canals remains unknown. Furthermore, it is uncertain what cross-sectional area results in wave quantities that provide the most clinically useful or physically accurate characterization of the middle ear. Because most area-estimation methods rely on the inverse discrete Fourier transform, they likely implicitly involve some form of spatial averaging. Notably, most published data and available commercial instrumentation assume an invariant ear-canal cross-sectional area, and the impact of this assumption on wave quantities measured in anatomical ear canals of varying geometry is unknown.

(2) *Fundamental differences between ear-canal wave quantities and immittance:* As briefly noted by Huang *et al.* (2000), ear-canal wave quantities do not uniquely characterize the middle ear. Instead, they describe the effect of the impedance mismatch between the ear canal and the middle ear on a propagating wave in the ear canal. For readers not overly familiar with wave and transmission-line theory, this distinction may not be immediately clear from the frequent description as reflected or absorbed sound pressure or energy—descriptions that, although accurate, can obscure the fact that wave quantities characterize the interaction between the ear canal and middle ear rather than the middle ear alone. The literature often seems to imply equivalency or at least fails to distinguish between middle-ear immittance and ear-canal wave quantities in terms of representing middle-ear properties. To illustrate the non-uniqueness of wave quantities in describing middle-ear properties more explicitly, middle ears and ear canals vary considerably in size and shape, and one does not uniquely define the other. Conceptually, a given middle ear could terminate ear canals of different geometry. Despite the status of these middle ears being exactly identical, their wave quantities differ markedly (Nørgaard *et al.*, 2024). Therefore, ear-canal wave quantities do not uniquely characterize the middle ear, and the ear-canal cross-sectional area fundamentally confounds and contributes to inter-subject variability of ear-canal wave quantities. The literature appears to have consistently emphasized the metrological advantages of ear-canal wave quantities while failing to clarify these fundamental limitations in terms of uniquely characterizing the middle ear.

(3) *Low-frequency wave quantities in the ear canal:* A fundamental goal of WAI is to provide a physical characterization of the middle ear and its mechanisms responsible for hearing. Therefore, quantifying the status of the middle ear based on reflections of sound waves by the tympanic membrane requires that this actually represents the underlying physical phenomenon. Although these reflections undoubtedly play a role at high frequencies, their role is questionable at low frequencies. At high frequencies, when a propagating wave is subject to a considerable phase shift along the ear canal, impedance mismatches occur both at its entrance (between the sound source and the ear-canal propagation medium) and termination (between the ear-canal propagation medium and the tympanic membrane) (Møller, 1992; Møller *et al.*, 1995). That is, a sound wave incident on the ear canal is subject to the ear-canal characteristic impedance rather than the ear-canal impedance, then propagates through the ear canal, and is finally reflected by the middle ear. Accurately characterizing the sound source, e.g., by its acoustic Thévenin-equivalent parameters, then enables distinguishing between reflections

from the source and the termination to intuitively express any acoustic quantity (e.g., pressure, volume velocity, or energy) absorbed or reflected by the middle ear as a proportion of the incident quantity having already entered the ear canal from the sound source. However, at low frequencies, when the wavelength is much longer than the ear canal, a propagating wave only experiences a negligible phase shift along the ear canal. That is, the sound pressure throughout the canal is approximately constant, and the pressure at its entrance effectively acts directly on the tympanic membrane. In other words, a sound wave incident on the ear canal is barely subject to the ear-canal characteristic impedance, and effectively only a single impedance mismatch is present between the sound source and the combined ear canal and middle ear. Thus, there is only a negligible intermediate state of an incident propagating wave between the sound source and middle ear to serve as a reference for quantifying a relative reflected or absorbed acoustic quantity. Calculating low-frequency ear-canal wave quantities from the measured ear-canal impedance when the combined ear canal and middle ear practically behaves as a lumped-element system with negligible wave propagation imposes the assumption that the sound source is a propagating wave with properties given by the characteristic impedance. This is of course not the case, and the interpretation of these wave quantities relates more to a theoretical reflection dictated by the ear-canal characteristic impedance used for their calculation than any physical behavior of the specific ear. This observation suggests that wave quantities do not physically characterize the middle ear and its role in low-frequency hearing.

(4) *Clinical applications of WAI:* An optimal quantity for characterizing the middle ear, both in research and in the clinic, should not be chosen solely based on its theoretical physical or signal-processing properties; practical considerations such as measurement accuracy and reproducibility are equally important. For clinical diagnosis, which often relies on pattern recognition—performed by trained professionals, statistical models, automated machine-learning algorithms, etc.—physical significance may be less important, and a suitable quantity may simply provide the best decision accuracy. Although current methods appear capable of accurately measuring ear-canal wave quantities (Nørgaard *et al.*, 2020), the measurement of middle-ear immittance is more challenging. Some researchers have estimated these quantities by propagating ear-canal immittance to the tympanic membrane using uniform (Rabinowitz, 1981; Voss and Allen, 1994; Huang *et al.*, 2000; Keefe *et al.*, 2015) and non-uniform (Lewis and Neely, 2015; Keefe, 2020; Merchant and Neely, 2021) transmission-line models with the ear-canal geometry estimated *in situ* from immittance or wave quantities. However, none of these models have been validated in scenarios where the middle-ear immittance is known, so the accuracy of the estimated middle-ear immittance in real ears remains unknown.

III. METHODS

A. Ear-canal simulations

For the purpose of illustrating the physical significance of wave quantities in the case of uniform sound fields in the ear canal, we simulated the ear-canal acoustics using lossless uniform one-dimensional transmission-line and lumped-element models, both terminated by the same middle-ear impedance Z_{me}. We modeled Z_{me} using two parallel Helmholtz resonators as described by Nørgaard *et al.* (2019b), approximating the termination impedance of a standardized occluded-ear simulator (IEC 60318-4, 2010).

For the transmission-line models, we calculated the ear-canal impedance,

$$Z_{\mathrm{ec}} = Z_0 \frac{Z_{\mathrm{me}} + jZ_0 \tan kl_{\mathrm{ec}}}{Z_0 + jZ_{\mathrm{me}} \tan kl_{\mathrm{ec}}}, \tag{6}$$

with the unit imaginary number j, the wavenumber $k = \omega/c$, and the ear-canal length l_{ec}. For the lumped-element ear canals, we simulated the ear-canal impedance Z_{ec} as the parallel combination of the middle-ear impedance Z_{me} and the lumped-element impedance of the ear-canal volume $V_{\mathrm{ec}} = S_{\mathrm{ec}} l_{\mathrm{ec}}$ (summing the corresponding admittances),

$$Z_{\mathrm{ec}} = \left(\frac{1}{Z_{\mathrm{me}}} + \frac{j\omega V_{\mathrm{ec}}}{\rho c^2} \right)^{-1}. \tag{7}$$

For each model Z_{ec}, we calculated the ear-canal reflectance R_{ec} and energy absorbance A_{ec} from Eqs. (3) and (4), respectively.

Given the assumption of a uniform lossless one-dimensional transmission line inherent to the concept of ear-canal wave quantities, we can estimate the middle-ear impedance $\hat{Z}_{\mathrm{me}}$ by removing the effects of the ear canal from the ear-canal impedance Z_{ec} using such a model,

$$\hat{Z}_{\mathrm{me}} = Z_0 \frac{jZ_0 \tan kl_{\mathrm{ec}} - Z_{\mathrm{ec}}}{jZ_{\mathrm{ec}} \tan kl_{\mathrm{ec}} - Z_0}. \tag{8}$$

Similarly, as practiced in conventional tympanometry, it is possible to estimate the middle-ear impedance $\hat{Z}_{\mathrm{me}}$ by removing the parallel lumped-element impedance of the ear-canal space from the ear-canal impedance Z_{ec} (subtracting the corresponding admittances),

$$\hat{Z}_{\mathrm{me}} = \left(\frac{1}{Z_{\mathrm{ec}}} - \frac{j\omega V_{\mathrm{ec}}}{\rho c^2} \right)^{-1}. \tag{9}$$

For our simulations, we applied Eqs. (8) and (9) to estimate the middle-ear impedance $\hat{Z}_{\mathrm{me}}$ only from the ear-canal impedance Z_{ec} simulated using a transmission line [Eq. (6)]. We simulated ear canals of cross-sectional area $S_{\mathrm{ec}} = 44.2\,\mathrm{mm}^2$ and lengths l_{ec} from 15 to 40 mm in 5 mm increments. Established general transmission-line theory conventionally considers wave effects

https://doi.org/10.1121/10.0043164

prudent to consider when the wavelength $\lambda < l_{ec}/10$. Here, we will refer to the frequency above which this condition is met as the critical frequency

$$f_c = \frac{c}{10 l_{ec}}. \tag{10}$$

B. 3D-printed middle-ear simulator and ear canals

1. Middle-ear simulator

To study the variation in wave quantities of different ear canals terminated by the same middle ear, we constructed a middle-ear simulator with an impedance representative of the human ear canal that allowed different ear canals to be attached. This approach is based on the underlying logical premise that measured acoustic quantities that are independent of the attached ear canal provide a unique characterization of the middle ear. The middle-ear simulator consisted of two parallel Helmholtz resonators, designed to resemble the termination impedance of a standardized occluded-ear simulator (IEC 60318-4, 2010) and the middle-ear impedance Z_{me} used for the simulations in Sec. III A.[2] The internal design of the Helmholtz resonators and acoustic resistors were identical to those used by Nørgaard (2023), although the distance between the two Helmholtz resonators was decreased to accommodate for narrower ear canals. Because of mechanical tolerances in the 3D-printing process, and, perhaps more importantly, because of a specified tolerance of ±20% in the resistance of the acoustic resistors, the true characteristics of the middle-ear simulator are unknown. The top of the middle-ear simulator featured a keyed interface to allow an ear canal with a reciprocal interface to be mounted and held in place by a matching threaded retaining nut. The flat contact surface of the middle-ear simulator ensured an acoustic seal with the attached ear canal, whereas an O-ring placed at the circumference of the contact surface provided a barometric seal. The backsides of the Helmholtz resonators were sealed by gluing two lids into place. Because of excessive oblique orientations of some of the 3D-printed ear canals relative to the plane of the tympanic annulus, the middle-ear simulator and retaining nut were designed such that the top of the retaining nut was flush with the middle-ear plane. Figure 1 depicts cross-sectional renderings of the middle-ear simulator with uniform and anatomical ear canals attached (described in Secs. III B 2 and III B 3, respectively). All 3D-printed parts were fabricated using a ProJet MJP 2500 Plus (3D Systems, Inc., Rock Hill, SC, USA) using the material Visijet M2S-HT90 (3D Systems, Inc., Rock Hill, SC, USA), an acoustically rigid plastic material similar to acrylonitrile butadiene styrene (ABS). The relative fabrication tolerance of the parts was specified as ±0.001–0.002 in. per inch printed material (0.1–0.2%).

2. Uniform ear canals

We constructed 3D-printed uniform ear canals with cross-sectional areas from 20 to 80 mm^2 in 10 mm^2 increments, approximately covering the range of areas frequently observed in adult ears (Voss *et al.*, 2025). The total length of the uniform ear canals was fixed at 25 mm, excluding the insertion depth of the ear probe, resulting in an effective length of approximately 20 mm. We did not vary the canal length for this study because its effect on WAI measurements was previously studied by Nørgaard *et al.* (2019a), although only for a single cross-sectional area.

3. Anatomical ear canals

Based on anonymized high-resolution computed-tomography (CT) scans, eleven anatomical ear canals were 3D-printed from the entrance (Balouch *et al.*, 2023), approximately representing the typical location of the ear-probe placement, further selected to be reasonably circular to allow for a leak-free insertion, to the tympanic annulus. These scans represent a subset of the 221-ear dataset described in Voss *et al.* (2025) from the ear-canal entrance to the tympanic annulus. For this study, six canals were selected from individuals aged 40–50 years, with cross-

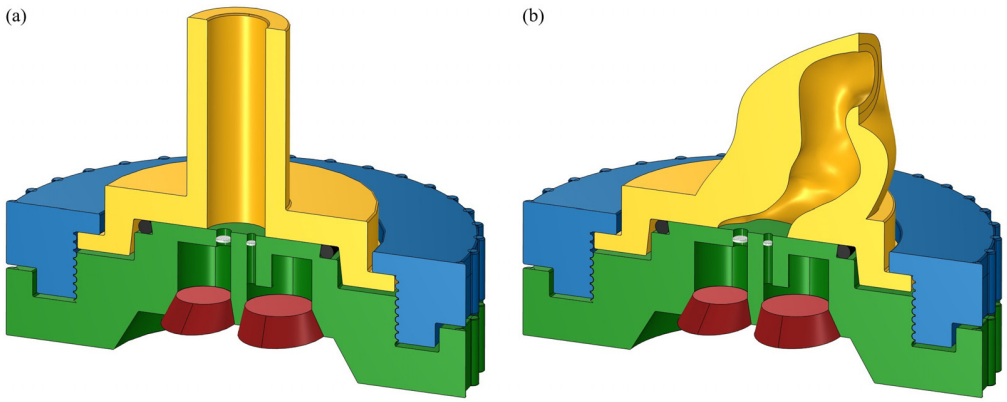

FIG. 1. Cross-sectional renderings of the 3D-printed middle-ear simulator with an attached (a) uniform ear canal and (b) anatomical ear canal obtained from a scanned human ear (ear 15153L, Table 1). Colors represent individual mechanical parts: (yellow) detachable ear canal, (blue) threaded retaining nut for securing the ear canal in place, (green) middle-ear simulator with Helmholtz resonators, (red) lids for sealing the backside of the Helmholtz resonators, (white) acoustic resistors for damping the Helmholtz resonance frequencies, and (black) sealing O-ring.

TABLE I. Properties of the 11 3D-printed anatomical ear canals constructed from the dataset of Voss *et al.* (2025), sorted by age, in terms of the ear ID; age; acoustic isosurface area near the ear probe $S_{ec}(d=0)$ (y-values for the rightmost points on each curve in Fig. 2); the estimated cross-sectional areas $\hat{S}_{ec}$ using the method of Nørgaard *et al.* (2019c); the average longitudinal isosurface area $\langle S_{ec}(d)\rangle_0^{l_{ec}}$ [see Eq. (13)]; the total acoustic lengths of the ear canals l_{ec} (x-values for the leftmost points on each curve in Fig. 2); and the acoustically estimated uniform ear-canal lengths $\hat{l}_{ec}$ [Eq. (11)] based on ear-canal reflectance calculated using Nørgaard *et al.* (2019c).

Subject details		Areas S_{ec} [mm^2]			Lengths l_{ec} [mm]	
Ear ID[a]	Age [years]	$S_{ec}(d=0)$	$\langle S_{ec}(d)\rangle_0^{l_{ec}}$	$\hat{S}_{ec}$	l_{ec}	$\hat{l}_{ec}$
6207L[b]	0.98	16.6	9.18	8.6	15.1	39.8
6466L	4.47	31.7	34.9	40.1	16.0	15.4
53L	15.9	99.6	66.8	67.4	25.8	27.3
27955948R[c]	19.9	53.2	48.0	23.0	28.6	30.7
10685L	41.41	63.8	42.6	43.2	28.1	26.5
15153L	42.85	58.1	41.9	45.9	23.8	24.2
10687R	43.13	86.7	48.8	46.4	26.3	24.5
61L	46.0	17.0	40.4	34.4	24.0	24.0
10714L	46.02	60.7	57.8	46.7	27.3	25.2
19L	47.0	94.8	48.6	48.0	25.4	22.8
15160L	73.0	47.6	39.4	38.6	12.8	13.2

[a]Identification (ID) number and side.
[b]Left (L).
[c]Right (R).

sectional areas at the first bend ranging from 42 to 92 mm^2. The remaining five canals were chosen to represent a broader variation in both age and cross-sectional area. Table I lists some relevant characteristics of the various anatomical ear canals.

A combination of software tools was used to prepare files for 3D printing the ear canals from the high-resolution CT scans (Feng, 2024). The process began with the open-source platform 3D SLICER,[3] where a stack of transverse Digital Imaging and Communications in Medicine (DICOM) images was loaded and converted to a 3D mesh representing the ear-canal airspace. The CT data were rendered volumetrically, and all airspaces were isolated using a threshold range of −1024 to −200 Hounsfield units (HU). The canal airspace was segmented using anatomical planes at the tympanic annulus and canal entrance,[4] isolated with the SCISSORS tool, and smoothed to remove small artifacts. The resulting air volume within the canal was exported as a 3D mesh in OBJ format. The mesh was then refined and prepared for printing. First, it was imported into MESHMIXER (Autodesk, Inc., San Francisco, CA, USA), where holes were filled using the MAKE SOLID function, and the model was exported again as an OBJ file. Finally, the open-source tool INSTANT MESHES[5] was used to convert the surface topology from triangular to quadrilateral meshes,[6] which was needed for the remaining steps. The quadrilateral meshes were imported into FUSION 360 (Autodesk, Inc., San Francisco, CA, USA) and converted into T-spline bodies to enable generation of inverse canal models for 3D printing. The solid body, representing the ear canal, was then inverted so that the canal became an internal air-filled volume; an enclosing body was created using the LOFT tool to surround the canal geometry, and a Boolean subtraction was performed to remove the ear-canal solid from this outer shell, producing its inverse. Because of the extensive manual process of generating 3D-printable anatomical ear canals from CT scans, we had to limit this study to 11 canals.

C. Ear-canal cross-sectional area functions

We extracted low-frequency one-dimensional acoustical ear-canal cross-sectional area functions of the anatomical ear canals using an approach based on a finite-element simulation of acoustic isosurfaces, i.e., surfaces of constant sound pressure. These acoustical area functions differ from the geometrical area functions reported by Voss *et al.* (2025) in that they describe area function experienced by the sound waves rather than planar cross-sectional slices. For this reason and to ensure that the utilized areas and ear-probe placement matched the 3D-printed parts as closely as possible, we chose to base our analyses (Sec. III D) on these acoustical area functions rather than the planar cross-sectional geometry from the canal entrance to the tympanic annulus reported by Voss *et al.* (2025). Figure 2 shows the extracted cross-sectional areas $S_{ec}(d)$ as a function of the longitudinal axis d for all 11 ear canals, approximately aligned to the location of the inserted ear probe. The isosurface area functions shown in Fig. 2 and a MATLAB script to generate are included in the supplementary material.

First, the solid-body ear-canal geometries were imported into COMSOL MULTIPHYSICS 6.3 (COMSOL, Inc., Burlington, MA, USA). Using the PRESSURE ACOUSTICS physics interface, a *NORMAL VELOCITY* boundary condition was applied to the planar entrance of the ear canal, whereas the remaining surfaces, including the planar tympanic annulus, were treated as rigid boundaries. The simulation was run at an arbitrary frequency of 100 Hz. This frequency was selected to be well below the half-wave standing-wave frequency, thereby ensuring the formation of fairly evenly distributed pressure isosurfaces along the ear canal because of a small but gradually increasing pressure along the canal. Compared to the wavelength of the analysis frequency, we defined a relatively fine mesh with an element size no greater than 2 mm and further refinement near curved features to improve the resolution of the exported isosurface geometry. For each ear canal, using the simulation at 100 Hz, 101 isosurfaces were defined along its length, with the first one intersecting the circumference of the ear-canal entrance and the last one intersecting the tympanic annulus. This ensured that all isosurfaces intersected only the ear-canal walls. Because our simulation utilized the default quadratic shape functions, regions between mesh vertices, which are most likely to intersect with the isosurfaces, are approximated using second-order polynomials. The tessellated isosurfaces were exported in VTU file format based on the open-source VIRTUALIZATION TOOLKIT[7] and imported into MATLAB R2025b (The MathWorks, Inc., Natick, MA, USA) using the open-source toolbox VTKTOOLBOX.[8] In MATLAB, the area of each

https://doi.org/10.1121/10.0043164

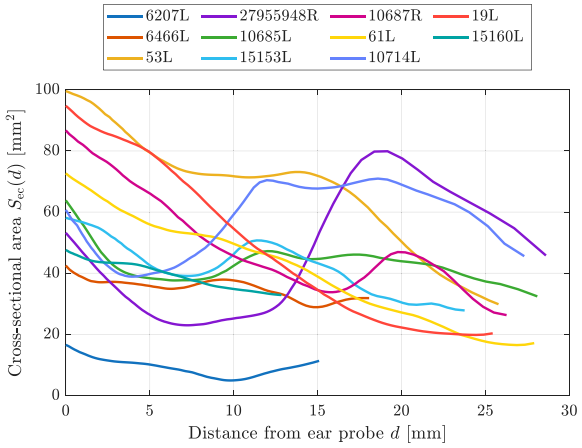

FIG. 2. The acoustical ear-canal cross-sectional area functions $S_{ec}(d)$, extracted from acoustic isosurfaces, as a function of the approximate longitudinal distance from the ear probe d of the ear canals of the various ear IDs listed in Table I. Note that these isosurface area functions differ from simple planar cross-sectional area functions in that they represent the non-uniform surface of the acoustic wavefront.

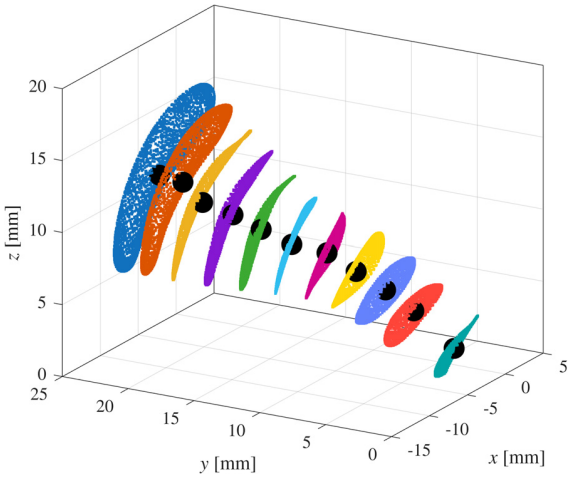

FIG. 3. Vertices for 11 of the 101 isosurfaces, indicated by individual colors, and isosurface center points, indicated by black points, for ear 19L. The point (0,0,0) represents the center of the tympanic annulus, which lies in the x-y plane. Note that the Cartesian coordinates (x, y, z) here differ from the longitudinal distance d from the entrance of the ear canal in Fig. 2.

isosurface was calculated by summing the areas of its constituent triangles. The center point of each isosurface was computed as the geometrical mean of all its vertices. To construct a longitudinal axis, the distances between adjacent isosurfaces were calculated as the norm of the difference between their center points. Figure 3 shows the isosurface vertices and center points for 11 of the 101 isosurfaces for ear 19L.

D. Equipment and measurements

The measurements reported in this study were performed using a FireFace UCX II (RME Audio, Haimhausen, Germany) sound card at a sampling frequency of 44.1 kHz. Data acquisition and playback were controlled through custom MATLAB scripts and the third-party utility PLAYREC.[9] A Titan-based ear probe (Interacoustics A/S, Middelfart, Denmark), modified for extended bandwidth and reduced crosstalk, was used for all measurements. Calibrations and measurements were conducted using an acoustic click stimulus, normalized to provide a flat zero-phase acoustic spectrum in the frequency range 0.1–20 kHz (although results are only shown in the range 0.25–16 kHz) into an anechoic waveguide of cross-sectional area 50.3 mm^2. For each measurement, 64 clicks were presented in blocks of 2048 samples, which were averaged to reduce noise.

To determine the acoustic Thévenin-equivalent parameters of the ear probe (the source pressure P_s and impedance Z_s), we used the calibration method and waveguides described by Nørgaard *et al.* (2017b). With the ear probe inserted into the various uniform and anatomical ear canals, each attached to the identical middle-ear simulator, the ear-canal impedance Z_{ec} was computed from the measured ear-canal pressure P_{ec} using Eq. (1). From each measured ear-canal impedance Z_{ec}, the corresponding ear-canal reflectances R_{ec} were calculated using the method described by Nørgaard *et al.* (2019c), which compensates for oblique ear-probe insertions. This method further implicitly compensates for evanescent modes and estimates the ear-canal characteristic impedance as the fitted ordinate intercept $\hat{Z}_{0,ec}$, from which the estimated cross-sectional area $\hat{S}_{ec} = \rho c/\hat{Z}_{0,ec}$. We also computed reflectance R_{ec} using the method of Voss and Allen (1994), assuming an invariant ear-canal cross-sectional area $\hat{S}_{ec} = 44.2\,\text{mm}^2$. In both cases, ear-canal absorbance A_{ec} was calculated from Eq. (4). To estimate the middle-ear impedance $\hat{Z}_{me}$, the measured ear-canal impedance Z_{ec} was propagated to the middle ear using Eq. (8) with the ear-canal length $\hat{l}_{ec}$ estimated from the reflectance phase delay τ_ϕ [Eq. (5)],

$$\hat{l}_{ec} = \langle \tau_\phi \rangle \frac{c}{2}, \tag{11}$$

where the angle brackets denote averaging, in this case across the frequency range 1–20 kHz.

For the anatomical ear canals, we further calculated ear-canal absorbance A_{ec} based on the acoustical cross-sectional area at the approximate location of the ear probe $S_{ec}(d = 0)$ in Table I. The ear-canal impedance was additionally propagated to the tympanic membrane using a lossless non-uniform transmission-line model composed of cascaded conical horn segments (Caussé *et al.*, 1984; Benade, 1988; Nørgaard *et al.*, 2019b). Based on the ear-canal transmission matrix with elements a_{11}, a_{12}, a_{21}, and a_{22}, calculated from the 101 acoustic isosurface areas and distances for ear canals described in Sec. III C, we estimated the middle-ear impedance as

$$\hat{Z}_{me} = \frac{a_{12} - a_{22}Z_{ec}}{a_{21}Z_{ec} - a_{11}}. \tag{12}$$

IV. RESULTS

A. Simulations of uniform transmission-line and lumped-element ear canals

This section presents results illustrating the physical significance of wave quantities based on the simulation approach described in Sec. III A. Figure 4 shows results from each of the simulated ear canals, using both uniform transmission-line and lumped-element models for different canal lengths l_{ec}. The shown quantities include the ear-canal-admittance Y_{ec} [Eqs. (6) and (7)] magnitudes and phases, ear-canal absorbances A_{ec} [Eq. (4)] and reflectance phase delays τ_ϕ [Eq. (5)], expressed as equivalent lengths $\tau_\phi c/2$, and estimated middle-ear-admittance $\hat{Y}_{me}$ [Eqs. (8) and (9)] magnitudes and phases in units of mmho[10] based only on the transmission-line Y_{ec}, including critical frequencies f_c [Eq. (10)].

For Y_{ec} magnitudes and phases in Figs. 4(a) and 4(d), respectively, the transmission-line and lumped-element models converge toward low frequencies, as expected. At f_c, some discernible discrepancy arises between the two models, which is however small compared to the divergence observed toward higher frequencies where standing waves become prominent. These results merely confirm and illustrate the well-known fact that ear-canal acoustics resulting from variations in ear-canal geometry strongly influence Y_{ec} and obscure the underlying middle-ear mechanics at higher frequencies but not at lower frequencies.

For A_{ec} and τ_ϕ in Figs. 4(b) and 4(e), respectively, quantities based on the transmission-line model naturally coincide, except for the expected length offsets in τ_ϕ, because both are otherwise independent of ear-canal length. However, similar to Y_{ec} in Figs. 4(a) and 4(d), A_{ec} and τ_ϕ based on the lumped-element model coincide with the transmission-line model at low frequencies but diverge progressively toward higher frequencies. The variation in A_{ec} between the two types of models at f_c appears greater relative to the variation at higher frequencies compared to that seen for Y_{ec} in Figs. 4(a) and 4(d). Notably, at low frequencies, A_{ec} and τ_ϕ using the two models are nearly identical. That is, in a lumped-element ear-canal model—where no wave propagation occurs—low-frequency wave quantities are almost identical to those in a one-dimensional transmission-line model that specifically simulates wave propagation. Note that, because the lumped-element models lack information on ear-canal length and cross-sectional area and, thereby, characteristic impedance, but only encodes the ear-canal volume, the simulated lumped-element ear canals representing various lengths equivalently correspond to different cross-sectional areas producing identical volumes. These results signify that, at low frequencies, the reflection of sound waves in the ear canal plays a negligible role, and wave quantities do not provide a meaningful physical characterization of the middle ear and the transduction mechanism underlying hearing. Instead, these wave quantities are arbitrarily determined by ear-canal characteristic impedance corresponding to the cross-sectional area. At high frequencies, the deviation between the two models merely suggests that wave propagation plays some kind of role in characterizing acoustic transduction of sound by the middle ear. Toward higher frequencies, both lumped-element A_{ec} and τ_ϕ approach zero because of the growing impedance mismatch between the characteristic impedance and the lumped-element ear-canal volume.

For $\hat{Y}_{me}$ magnitudes and phases shown in Figs. 4(c) and 4(f), respectively, the lumped-element and transmission-line

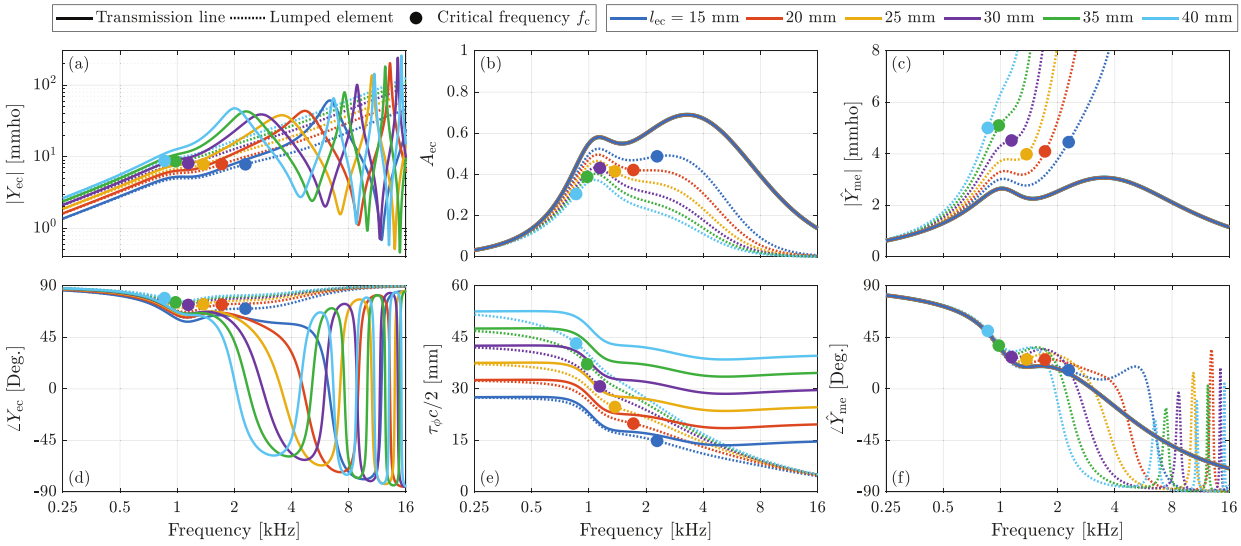

FIG. 4. A comparison between simulated (solid lines) transmission-line and (dotted lines) lumped-element ear canals terminated by identical middle-ear admittances for (individual line colors) various ear-canal lengths l_{ec} and the cross-sectional area $S_{ec} = 44.2\,\text{mm}^2$, including (circular markers) critical frequencies f_c [Eq. (10)]. The shown quantities include the ear-canal-admittance Y_{ec} [Eqs. (6) and (7)] (a) magnitudes and (d) phases; ear-canal (b) absorbances A_{ec} [Eq. (4)] and (e) reflectance group delays τ_ϕ [Eq. (5)], expressed as equivalent lengths $\tau_\phi c/2$; and estimated middle-ear-admittance $\hat{Y}_{me}$ [Eqs. (8) and (9)] (c) magnitudes and (f) phases based only on the transmission-line Y_{ec}. Note that A_{ec} and $\hat{Y}_{me}$ for all l_{ec} are identical for the transmission-line models. Deg., degree.

https://doi.org/10.1121/10.0043164

models converge at lower frequencies, as expected. The two types of models start to deviate substantially between 0.5 and 2 kHz, depending on ear-canal length. This illustrates the limitations of a lumped-element model in approximating and compensating for the effects of the ear canal simply based on its volume and why conventional 1-kHz tympanometry should only be used for tiny ear canals. Transmission-line $\hat{Y}_{\mathrm{me}}$ all coincide because they were propagated to the plane of the tympanic membrane using the same transmission-line models used for calculating the ear-canal admittance Y_{ec}. Thus, these $\hat{Y}_{\mathrm{me}}$ are identical to the true middle-ear admittance Y_{me}.

B. Measurements in uniform ear canals terminated by the same middle ear

This section presents results comparing measurements in the uniform ear canals of various cross-sectional areas terminated by the same middle-ear simulator described in Secs. III B 2 and III B 1, respectively. For each cross-sectional area, Fig. 5 shows ear-canal absorbances A_{ec} [Eq. (4)], reflectance phase delay τ_ϕ [Eq. (5)], expressed as equivalent lengths $\tau_\phi c/2$, and estimated middle-ear-admittance $\hat{Y}_{\mathrm{me}}$ [Eq. (8)] magnitudes and phases using a uniform transmission-line model, calculated from measurements of ear-canal impedance Z_{ec} [Eq. (1)]. Results are shown using the method of Nørgaard *et al.* (2019c) in the left column of panels in Fig. 5, which implicitly estimates the ear-canal cross-sectional area $\hat{S}_{\mathrm{ec}}$, and Voss and Allen (1994) in the right column of panels in Fig. 5, using the invariant area $\hat{S}_{\mathrm{ec}} = 44.2\,\mathrm{mm}^2$ for calculating the various quantities. Corresponding colors in all panels of Fig. 5 are based on the same measured Z_{ec}. The results shown in Fig. 5 and a MATLAB script to generate are included in the supplementary material.

Using the method of Nørgaard *et al.* (2019c), the variation in A_{ec} in Fig. 5(a) clearly illustrates how S_{ec} confounds the ability of A_{ec} and other wave quantities to uniquely characterize the middle ear in this ideal case of a uniform ear canal. The same middle ear produces markedly different values of A_{ec} depending on S_{ec} of the ear canal that it terminates, with A_{ec} scaled approximately inversely proportional to S_{ec} up to approximately 8 kHz. At frequencies above 8 kHz, additional factors begin to influence the measurements, including what is presumably small ear-probe calibration instabilities, propagating higher-order modes, and the non-uniform distribution of the middle-ear admittance across the terminating surface. The reflectance phase delays τ_ϕ in Fig. 5(c), on the other hand, are similar and nearly constant beyond the first middle-ear resonance frequency at 1 kHz and correspond approximately to the nominal ear-canal length of 20 mm. Below 1 kHz where the middle-ear volume contributes with a simple compliance in parallel with the ear-canal volume, the smaller S_{ec} causes an increased delay. In contrast, the estimated $\hat{Y}_{\mathrm{me}}$ in Figs. 5(e) and 5(g) are remarkably consistent up to 6 kHz. This consistency suggests that accurate estimates of both $\hat{S}_{\mathrm{ec}}$ and ear-canal lengths $\hat{l}_{\mathrm{ec}}$ [Eq. (11)] were achieved across the various uniform ear canals. The relative errors of all $\hat{S}_{\mathrm{ec}}$ were below 5.2% from their nominal values, with a mean relative error of 4.3%. These results also suggest that, given accurate knowledge of the ear-canal geometry, it may be possible to uniquely characterize the middle ear by estimating $\hat{Y}_{\mathrm{me}}$. At frequencies above 6 kHz, even in this idealized case of uniform canals, only small calibration, measurement, and geometry errors may be responsible for the increased variability in the estimated $\hat{Y}_{\mathrm{me}}$. Although the true admittance of the middle-ear simulator Y_{me} is not known, the bounds of $\hat{Y}_{\mathrm{me}}$—which are very similar to the transmission-line $\hat{Y}_{\mathrm{me}}$ in Fig. 4(c)—are the closest we can get to the true value of Y_{me}.

For the results using the method of Voss and Allen (1994) assuming an invariant $\hat{S}_{\mathrm{ec}}$ in Fig. 5(b), A_{ec} exhibits less variation at frequencies below and more variation at frequencies above approximately 2 kHz compared to Fig. 5(a). These results affirm the observation in Sec. IV A that, in the presence of a nearly uniform sound field with negligible propagating waves, the ear canal and middle ear effectively act as a lumped boundary with a single impedance mismatch from the sound source, and A_{ec} is solely determined by the assumed invariant $\hat{S}_{\mathrm{ec}}$. At higher frequencies where propagating waves gradually start to form, the variation in A_{ec} increases because it includes reflections from both the impedance mismatch between the source (defined by the incorrect assumed characteristic impedance) and the ear-canal propagation medium, and between the propagation medium and the middle ear. Naturally, the frequency at which this variation becomes pronounced depends chiefly on the ear-canal length l_{ec}, so the 2-kHz threshold observed here is specific to the lengths used in this study. From Fig. 5(d), however, it is evident that differences in total ear volume are directly translated into corresponding offsets in τ_ϕ below this 2 kHz limit. The excessive variation in the estimated $\hat{Y}_{\mathrm{me}}$ in Figs. 5(f) and 5(h) results both directly from the incorrect invariant $\hat{S}_{\mathrm{ec}}$ and indirectly from errors in the estimated $\hat{l}_{\mathrm{ec}}$ using Eq. (11) because of $\hat{S}_{\mathrm{ec}}$.

C. Measurements in anatomical ear canals terminated by the same middle ear

This section presents results comparing measurements in the 11 anatomical ear canals terminated by the same middle-ear simulator, described in Secs. III B 3 and III B 1, respectively, and listed in Table I. The left and middle columns of panels in Fig. 6 show quantities and conditions identical to Fig. 5. Figures 6(c) and 6(f) further show absorbances A_{ec} and reflectance phase delays τ_ϕ, expressed as equivalent lengths $\tau_\phi c/2$, respectively, calculated based on the acoustic isosurface area at the approximate location of the ear probe $S_{\mathrm{ec}}(d=0)$, listed in Table I. Figures 6(i) and 6(l) show the middle-ear-admittance $\hat{Y}_{\mathrm{me}}$ [Eq. (12)] magnitudes and phases, respectively, estimated using individual acoustic isosurface area functions $S_{\mathrm{ec}}(d)$ shown in Fig. 2. In addition, Table I further lists the estimated cross-sectional areas $\hat{S}_{\mathrm{ec}}$ of the anatomical ear canals using the method of Nørgaard *et al.* (2019c). The results shown in Fig. 6 and a

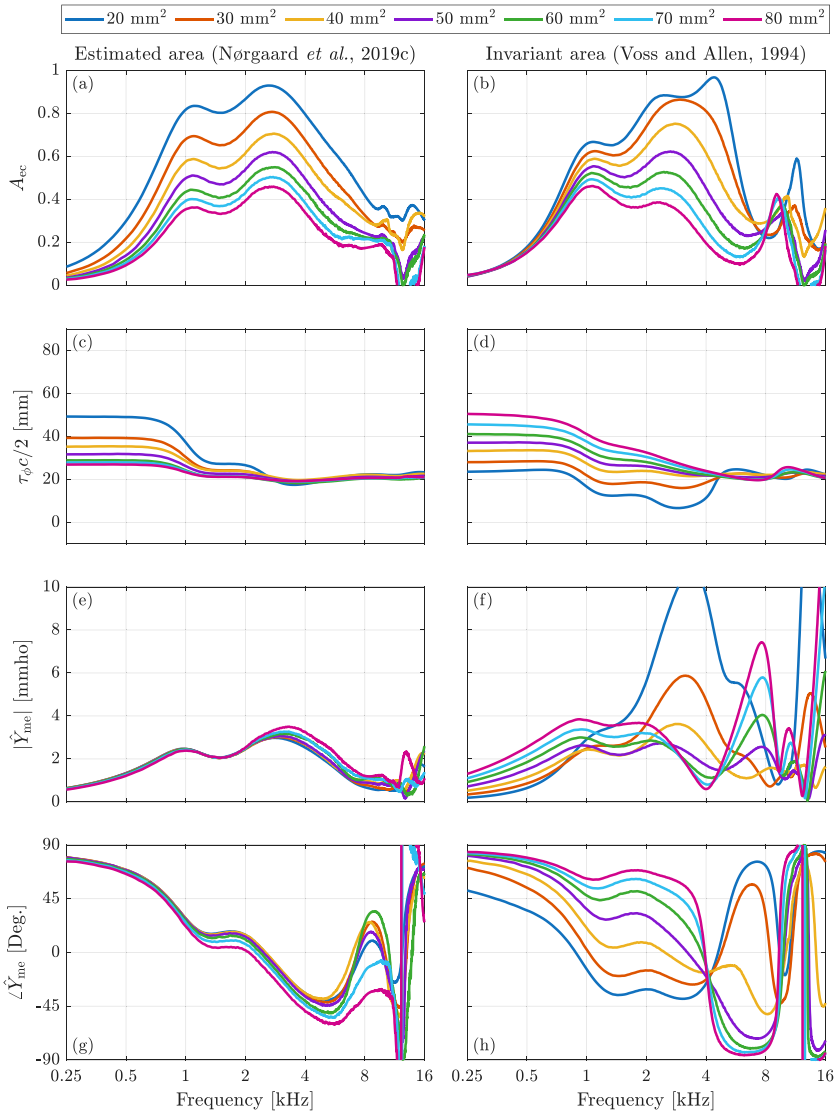

FIG. 5. Measurement results from the uniform ear canals of different cross-sectional areas and approximate lengths of 20 mm, terminated by the same middle-ear simulator. The (a), (b) absorbances A_{ec} [Eq. (4)]; (c), (d) reflectance phase delays τ_ϕ [Eq. (5)], expressed as equivalent lengths $\tau_\phi c/2$; and estimated middle-ear-admittance $\hat{Y}_{me}$ [Eq. (8)] (e), (f) magnitudes and (g), (h) phases using a uniform transmission-line model. Results are shown using the methods of (a), (c), (e), (g) Nørgaard *et al.* (2019c) in the left column of panels, which implicitly estimates the cross-sectional area $\hat{S}_{ec}$; and (b), (d), (f), (h) Voss and Allen (1994) in the right column of panels, assuming the invariant cross-sectional area of $\hat{S}_{ec} = 44.2\,\text{mm}^2$.

MATLAB script to generate are included in the supplementary material.

For the measured A_{ec} and τ_ϕ using the method of Nørgaard *et al.* (2019c) in Figs. 6(a) and 6(d), respectively, the variation generally aligns with what one might expect based on the results in Figs. 5(a) and 5(c) and the anatomical ear-canal areas in Fig. 2. Because ear 6207L has a tiny cross-sectional area (Fig. 2), it has an absorbance close to unity across many frequencies and larger delay at low frequencies. In most anatomical ear canals, as well as in the uniform canals in Fig. 5(a), the second absorbance peak near 3.3 kHz is consistently larger than the first peak near 1 kHz. However, in ear 27955948R, the absorbance spectrum exhibits a notable skewing of the peak heights, perhaps because of its particularly non-uniform area-distance function (Fig. 2) causing partial reflections along the canal.

For A_{ec} and τ_ϕ calculated using the method of Voss and Allen (1994) using the invariant cross-sectional area $\hat{S}_{ec} = 44.2\,\text{mm}^2$ in Figs. 6(b) and 6(e), respectively, the variation in A_{ec} is notably reduced below 3 kHz—even to a point where it is lower than in Fig. 5(b). Again, variations in ear-canal volume result directly in offsets in τ_ϕ at low frequencies in Fig. 6(e). At frequencies above 4–5 kHz, standing-wave effects become more prominent, resulting in local extrema in A_{ec}. In Fig. 6(a) using estimated cross-sectional areas, these high-frequency peaks are significantly reduced, producing much smoother absorbance curves, presumably because of the improved matching between the estimated and geometrical areas.

Disregarding ear 6207L, the variation in A_{ec} and τ_ϕ based on the cross-sectional area near the ear probe $S_{ec}(d = 0)$ in Figs. 6(c) and 6(f), respectively, appears to be generally greater than in any of the two preceding cases. This might be because of the generally larger cross-sectional areas near the ear probe relative to the remaining geometry, as Fig. 2 suggests, the longitudinal average of which generally correlates well with the assumed $\hat{S}_{ec} = 44.2\,\text{mm}^2$. For ear 6207L, however, the longitudinally averaged cross-sectional area is much smaller than at the ear-probe location, of which the latter is closer to the assumed $44.2\,\text{mm}^2$ in Fig. 6(b).

https://doi.org/10.1121/10.0043164

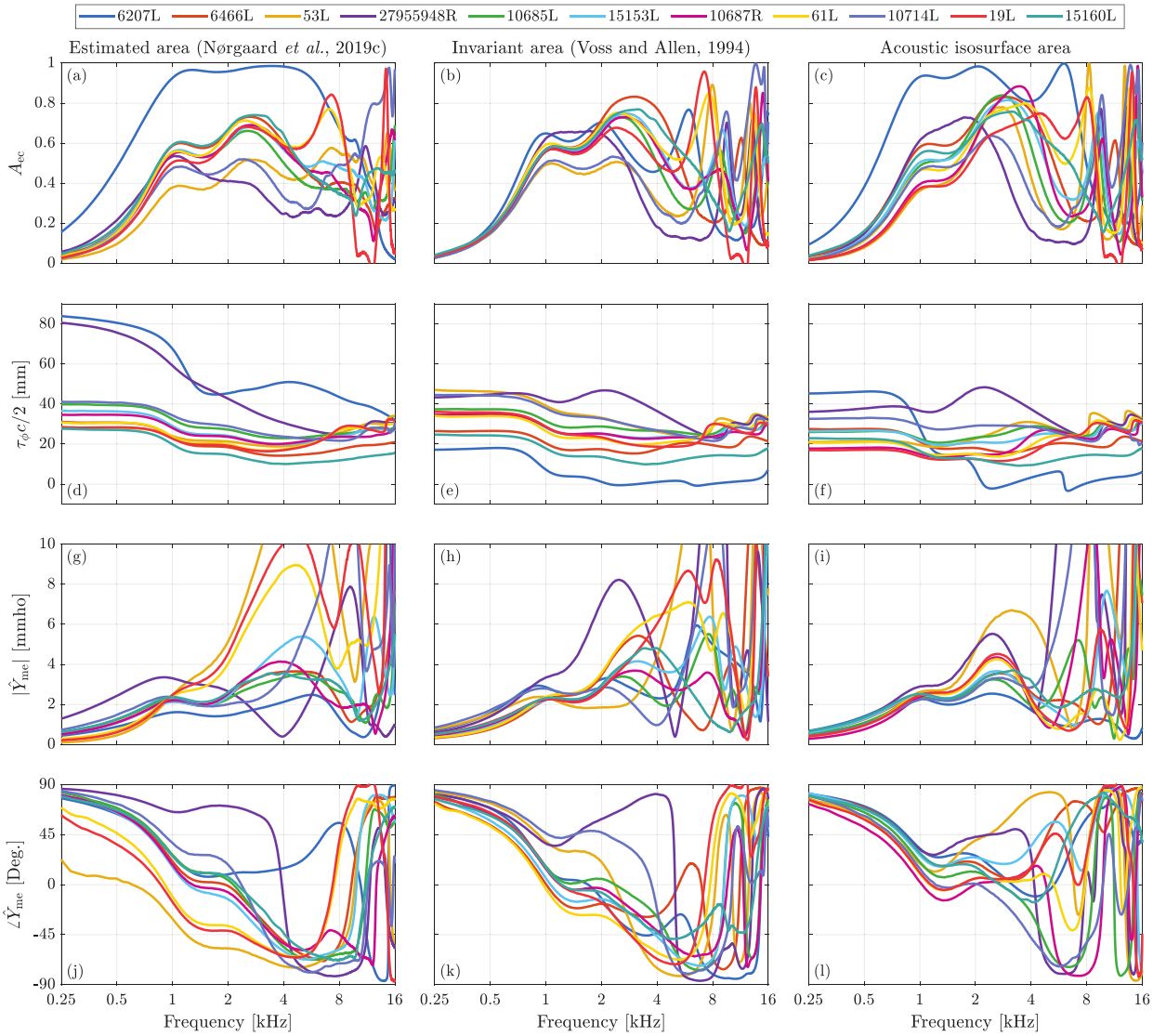

FIG. 6. Measurement results from the various anatomical ear canals terminated by the same middle-ear simulator listed in Table I. The (a), (b), (c) absorbances A_{ec} [Eq. (4)]; (d), (e), (f) reflectance phase delays τ_ϕ [Eq. (5)], expressed as equivalent lengths $\tau_\phi c/2$; and estimated middle-ear-admittance Y_{ec} (g), (h), (i) magnitudes and (j), (k), (l) phases. Results are shown using (g), (h), (j), (k) uniform [Eq. (8)] and (i), (l) non-uniform [Eq. (12)] transmission-line models; and using (a), (d), (g), (j) the method of Nørgaard *et al.* (2019c) in the left column of panels, which implicitly estimates the cross-sectional area $\hat{S}_{ec}$; (b), (e), (h), (k) using the method of Voss and Allen (1994) in the middle column of panels, assuming the invariant cross-sectional area of $\hat{S}_{ec} = 44.2\,\text{mm}^2$; and using (c), (f) the ear-canal cross-sectional area at the ear probe $S_{ec}(d = 0)$ and (i), (l) the ear-canal area functions $S_{ec}(d)$ (Fig. 2), based on acoustic isosurfaces, in the right column of panels. L, Left; R, Right; Deg., degree.

These results suggest that wave quantities measured using the acoustically estimated area [Fig. 6(a)] or the acoustical area near the ear probe [Fig. 6(c)], although likely providing a more physically accurate representation of sound-wave reflections by the middle ear, introduce considerable inter-subject variability in terms of uniquely representing middle-ear status because of anatomical differences in ear-canal geometry. In contrast, wave quantities measured using an invariant cross-sectional area [Fig. 6(b)], although not descriptive of any underlying physical phenomenon in the ear canal, yields wave quantities that are less influenced by anatomical variations in ear-canal geometry and may be better suited for clinical diagnosis of middle-ear disorders.

For the estimated middle-ear admittances $\hat{Y}_{me}$ [Eq. (8)] using the methods of Nørgaard *et al.* (2019c) and Voss and Allen (1994), shown in Figs. 6(g) and 6(j) and 6(h) and 6(k), respectively, the variation in $\hat{Y}_{me}$ appears substantial—likely to a degree that makes it less useful compared to absorbance for clinical diagnostics. These results suggest that a uniform transmission-line model may be insufficient to reliably estimate the middle-ear admittance across a broad frequency range, or, at the very least, that more representative estimates of ear-canal geometry are needed for this purpose. For $\hat{Y}_{me}$ estimated using the non-uniform transmission-line model in Figs. 6(i) and 6(l), some variation is expected; the acoustical cross-sectional area functions do not include the ear-canal portion near the tympanic annulus, for which the volume varies among ear canals, and the

exact ear-probe placements relative to the cross-sectional area functions are not known. Nonetheless, although the variation in $\hat{Y}_{\mathrm{me}}$ below 2 kHz is relatively small, it is still quite noticeable compared to Figs. 5(e) and 5(g), and the variation above 2 kHz seems disproportionately large despite being based on the individual acoustical cross-sectional area functions from Fig. 2.

To investigate the physical significance of the estimated cross-sectional areas $\hat{S}_{\mathrm{ec}}$ in the anatomical ear canals, we calculated the relative area errors as

$$\eta_S(d_r) = \left| 1 - \frac{\hat{S}_{\mathrm{ec}}}{\langle S_{\mathrm{ec}}(d) \rangle_0^{d_r l_{\mathrm{ec}}}} \right|, \tag{13}$$

between the estimated cross-sectional areas $\hat{S}_{\mathrm{ec}}$, shown in Table I, and the cross-sectional area functions $S_{\mathrm{ec}}(d)$, shown in Fig. 2, cumulatively averaged long their lengths l_{ec}. However, because the ear canals have different l_{ec} (the maximum longitudinal coordinate for individual ear canals in Fig. 2), $S_{\mathrm{ec}}(d)$ were cumulatively averaged along the relative longitudinal coordinate $d_r = d/l_{\mathrm{ec}}$ of the individual ear canals. Because the acoustic isosurfaces were not equidistantly spaced, the cumulative average ear canal areas were calculated by simple linear interpolation and numerical trapezoidal integration. Figure 7 shows this relative area error $\eta_S(d_r)$ for individual ear canals and averaged across ear canals, and Table I further lists the averaged isosurface areas $\langle S_{\mathrm{ec}}(d) \rangle_0^{l_{\mathrm{ec}}}$ along the entire ear-canal length l_{ec}. The results suggest that, both on an individual and averaged level, the acoustically estimated cross-sectional areas $\hat{S}_{\mathrm{ec}}$ using the method of Nørgaard *et al.* (2019c) do not approximate the cross-sectional area at the location of the ear probe, where the average relative error is just above 33%, but seem to approximate more the averaged cross-sectional area along the ear-canal length reaching a much lower relative error of approximately 13%, although somewhat larger than the mean relative area error for the uniform ear canals of 4.3%.

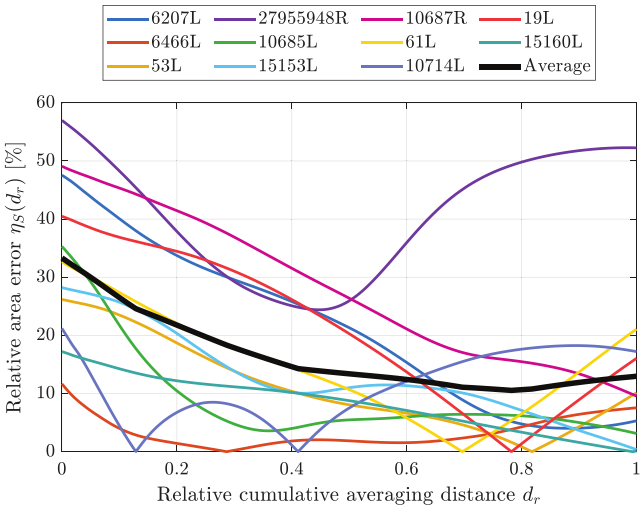

FIG. 7. The relative area error $\eta_S(d_r)$ [Eq. (13)] derived from measurements in the anatomical ear canals using the method of Nørgaard *et al.* (2019c) as a function of the cumulative averaging distance along the relative longitudinal dimension d_r for (colored lines) individual ear canals and (black line) averaged across ear canals. L, Left; R, Right.

V. DISCUSSION

A. Ear-probe placement and ear canals

Because our 3D-printed anatomical ear canals are rigid, there is likely some difference in the ear-probe placements from the corresponding human ear canals in a clinical setting, which are more malleable. Additionally, in a few cases, we were unable to fully insert the ear tip into the anatomical ear canals, even with the smallest available ear tip, and the ear probe was therefore manually held in place at the entrance until a leak- and noise-free measurement had been obtained. In human ear canals, various strategies can be employed to alter the ear-canal shape while placing the ear probe, such as pulling the pinna. In addition, the placement of the ear probe itself might alter the ear-canal geometry and the resulting acoustic measurements. Although current rapid-prototyping technology does allow constructing mechanical parts with properties similar to human tissue, this approach would require an extensive validation of the properties of these materials and identifying not only the ear-canal space but additionally the substances, i.e., bone, tissue, cartilage, and skin, in the vicinity of the ear canal from the CT scans. For this reason, we chose the approach using rigid ear canals for this study.

The estimated ear-canal cross-sectional area using Nørgaard *et al.* (2019c) appears to approximate the ear-canal cross-sectional areas, averaged along the longitudinal axis. It is important to emphasize that other methods for estimating this area (e.g., Keefe *et al.*, 1992; Rasetshwane and Neely, 2011; Nørgaard *et al.*, 2017a), depending on the frequency bandwidth, may approximate something else. Particularly, methods based on wider bandwidths may approximate the ear-canal cross-sectional area closer to the ear probe. Although soft ear-canal walls may affect ear-canal admittance and wave quantities, they may also affect the estimation of the ear-canal cross-sectional area. Soft ear-canal walls inherently absorb sound, which of course directly affects immittance and wave quantities. However, soft walls might alleviate effects of standing waves on wave quantities based on an invariant cross-sectional area, potentially increasing the approximate 3-kHz frequency limit.

B. Estimating middle-ear admittance

Although we were able to consistently estimate identical middle-ear admittances across our uniform ear canals of different cross-sectional areas, our results suggest that a uniform transmission-line model is inadequate for reliably estimating middle-ear immittance across a wider bandwidth in anatomical ear canals. At least, more representative estimates of ear-canal cross-sectional area and length are required for the transmission-line model than those estimated using our utilized acoustic methods. Furthermore, despite the rigidity of our anatomical ear-canal walls, we were unable to reliably estimate the middle-ear admittance

https://doi.org/10.1121/10.0043164

using the acoustical cross-sectional area functions of the individual ear canals. The exact ear-probe placements relative to the cross-sectional area functions are not known, and these area functions do not include the portion of the ear canal immediately adjacent to the tympanic membrane. This result suggests (1) that acoustic isosurface area functions with exact reference to the ear-probe placement are required to reliably estimate middle-ear immittance at higher frequencies, (2) that the interaction between the ear canal and tympanic membrane needs to be taken into account, or (3) that a one-dimensional non-uniform transmission-line model is entirely inadequate for estimating middle-ear immittance, perhaps because of effects near ear-canal bends that cannot be represented by a one-dimensional model (Hudde and Schmidt, 2009; Xia *et al.*, 2024). Additionally, in real ears, the middle-ear immittance is likely non-uniformly distributed across the surface of the tympanic membrane. In our case, this immittance is constituted by the two small openings leading to the Helmholtz resonators across an otherwise rigid planar surface, likely introducing some difference in the sound field near the middle-ear compared to the corresponding real ears.

C. Optimal quantities for clinical middle-ear diagnosis

In our interpretation of the results, among our considered quantities and methods, the assumption of an invariant cross-sectional area representative of adult ear canals (Voss and Allen, 1994) for calculating wave quantities provides the representation of middle-ear mechanics most suitable for middle-ear diagnostics in the clinic below approximately 3 kHz. These wave quantities provided less variation among our anatomical ear canals up to this frequency compared to our remaining considered quantities and methods. However, when the cross-sectional area of individual ear canals differ from the assumed value, wave quantities using an invariant cross-sectional area physically characterize neither the ear-canal sound field nor middle-ear mechanics but rather the theoretical reflection of sound waves because of the additional impedance mismatch at the location of the ear probe imposed by the assumed invariant cross-sectional area. This lack of physical significance means that one should exercise caution when interpreting these quantities because they do not characterize any physical features of the individual ear unless the assumed invariant and geometrical areas match. It also means that it likely makes no clinical difference whether the middle-ear status is assessed using wave quantities describing sound energy, pressure, or something else. It is of course plausible that wave quantities calculated from the estimated cross-sectional area, despite the confounding effects of this area, may be more suitable for diagnosing potential middle-ear pathologies that manifest themselves at frequencies beyond 3 kHz, where standing waves start to introduce substantial errors into wave quantities calculated using an invariant area. The approximate 3 kHz frequency limit determined here is principally dictated by the onset of standing waves in our relatively small population of 3D-printed anatomical ear canals, causing wave quantities based on an invariant cross-sectional area to vary more than those based on the estimated cross-sectional area. Because a large-scale extension of our current study would be extremely time-consuming, it might be possible to determine a more precise limit using a larger population of ear canals based on simulations utilizing a non-uniform transmission-line model rather than acoustic measurements.

For illustrating and understanding certain mathematical properties of normalized impedance and reflectance, it can be helpful to visualize these quantities on the Riemann sphere (Allen, 2020), which is the inverse stereographic projection of the extended complex plane onto a sphere. Mathematically, Eq. (3) is a bilinear (or Möbius) transformation on the simple form,

$$w = \frac{z-1}{z+1}, \tag{14}$$

acting on the normalized impedance, that rotates individual points on the Riemann sphere 90° around the axis spanning from $-j$ to j. Thus, for the input impedance of any passive system normalized by a real frequency-independent characteristic impedance, it transforms a complex number z on the positive real Riemann hemisphere $\mathrm{Re}\, z \geq 0$ to another complex number w on the lower Riemann hemisphere $|w| \leq 1$. For the ideal case of a lossless uniform transmission line with frequency-independent termination impedance that exceeds the characteristic impedance, individual points of normalized impedance on the Riemann sphere are rotated $2kl_{\mathrm{ec}}$ radians around the axis spanning from -1 to 1. The characteristic impedance exceeding the termination impedance changes the direction of the rotation. This means that singularities and the complex-harmonic kl_{ec} dependency inherent to impedance are transformed into equal reflectance magnitudes with linear phase. However, if impedance is not appropriately normalized, the rotation of normalized impedance is skewed, thus producing harmonic reflectance magnitudes.

For the sake of illustrating this rather non-trivial concept, Fig. 8 shows projections of simulated normalized acoustic impedance Z_{ec}/Z_0, with impedance Z_{ec} calculated based on Eq. (6), and reflectance R_{ec} [Eq. (3)] onto the Riemann sphere with $Z_{\mathrm{me}} = Z_0\left(\sqrt{2}+1\right)$, resulting in the nominal reflectance magnitude $|R_{\mathrm{ec}}| = \sqrt{2}-1$ for 25 values of kl_{ec} in equidistant steps from 0 to π (a full rotation). To illustrate the effects of using the correct characteristic impedance for impedance normalization, Fig. 8(a) shows projections for different scaling factors K applied to Z_0 both for the impedance calculation and normalization,

$$\frac{Z_{\mathrm{ec}}}{Z_0} = K\frac{\left(\sqrt{2}+1\right)+jK\tan kl_{\mathrm{ec}}}{K+j\left(\sqrt{2}+1\right)\tan kl_{\mathrm{ec}}}, \tag{15}$$

with K thus representing the factor of change in ear-canal cross-sectional area. The origins for $kl_{\mathrm{ec}} = 0$ are the intersections with the real circle on the upper Riemann

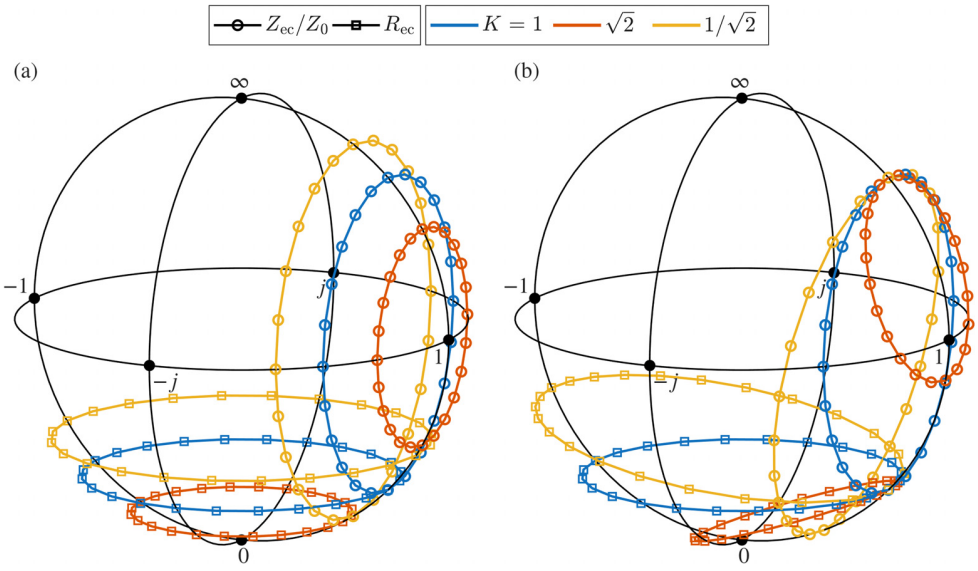

FIG. 8. Projections of (circles) normalized acoustic impedance Z_{ec}/Z_0, calculated based on Eq. (6), and (squares) reflectance R_{ec} [Eq. (3)] of a lossless uniform transmission line onto the Riemann sphere for 25 values of kl_{ec} in equidistant steps from 0 to π. To illustrate the effects of using the correct and an invariant characteristic impedance for impedance normalization, results are shown for (individual colors) different scaling factors K applied to Z_0 (a) both for the impedance calculation and normalization [Eq. (15)], and (b) only for impedance calculation and not normalization [Eq. (16)], respectively.

hemisphere $|z| > 1$. As expected, the result is three circles that are all parallel to but differently offset relative to the complex circle, with points equidistantly spaced. When rotated using the bilinear transform yielding reflectance R_{ec} [Eq. (3)], they produce constant but different magnitudes for the various K with linear identical phases $\angle R_{ec}$ (constant phase and group delays), evident from the equidistant spacing. To illustrate the effects of using an invariant characteristic impedance for impedance normalization, Fig. 8(b) shows projections for different K applied to Z_0 only for the impedance calculation but not for normalization,

$$\frac{Z_{ec}}{Z_0} = \frac{(\sqrt{2}+1) + jK \tan kl_{ec}}{K + j(\sqrt{2}+1)\tan kl_{ec}}, \tag{16}$$

with K thus representing the relative error between the geometrical and assumed cross-sectional area. As is evident, projections now intersect when kl_{ec} is an integer multiple of π for all K, but circles of Z_{ec}/Z_0 are skewed relative to the imaginary circle for non-unity K, resulting in non-constant $|R_{ec}|$. In addition, points are no longer equidistantly spaced for non-unity K, producing non-linear $\angle R_{ec}$. Most importantly, Z_{ec} of ear canals of varying geometry but adequately small kl_{ec} are transformed into similar $|R_{ec}|$. Notice also the difference in spacing between individual points for different K near small kl_{ec}, illustrating how information on ear-canal volume, affecting both impedance magnitude and phase, are transformed to only affect reflectance phase at low frequencies. The MATLAB script used for generating Fig. 8 is provided in the supplementary material. The ability to rotate the Riemann sphere and projections enhances the understanding of the concept.

The similarity in projected normalized impedance and reflectance for small kl_{ec} in Fig. 8(b) illustrates how the assumption of an invariant cross-sectional area when calculating wave quantities serves the important purpose of uniquely characterizing the middle ear while removing the effects of ear-canal geometry from wave-quantity magnitudes in the absence of standing waves at low frequencies—without the need to determine the ear-canal volume. That is, the rotation on the Riemann sphere transforms complex impedances (normalized by an invariant characteristic impedance), in which middle-ear and ear-canal characteristics are intertwiningly encoded into both magnitude and phase, into complex reflectances, where middle-ear characteristics shape only the magnitudes, which are clinically decipherable. Note that the impedance normalization based on the invariant cross-sectional area forces the normalized-impedance data to visually cluster when projected onto the Riemann sphere. When visualized using conventional magnitudes and phases, or real and imaginary parts as a function of frequency, the data do not cluster. It is the rotation on the Riemann sphere using the bilinear transformation that forces the reflectance magnitudes to cluster. This, however, is at the expense of the loss of characterization of the reflection of sound waves in the ear canal and significant confounding effects of standing waves at higher frequencies. Exactly determining the ear-canal volume is at least required to remove its effects from the ear-canal immittance at low frequencies, and doing so still introduces considerable errors into the estimated middle-ear admittance at frequencies as low as the critical frequency [Figs. 4(c) and 4(f)]. Feeney *et al.* (2013) suggested that research should focus more on temporal characteristics of WAI; however, because information on ear-canal volume primarily shapes these temporal characteristics of reflectance at lower frequencies when using an invariant cross-sectional area, this might prove counterproductive. Reflectance errors in human ears when

https://doi.org/10.1121/10.0043164

using an invariant cross-sectional area are not merely the result of the magnitude of kl_{ec} but, among other things, further depend on the middle-ear impedance Z_{me}, which defines the starting point on the Riemann sphere for $kl_{ec} = 0$, and the mismatch between assumed and actual areas, which defines the trajectory of the circle on the Riemann sphere. Still, deep ear-probe insertions certainly seem favorable to minimize kl_{ec}. It is important to emphasize the trivial property and caveat that wave-quantity magnitudes are mathematically non-unique because the middle-ear impedances Z_{me} and Z_0^2/Z_{me} produce identical wave-quantity magnitudes. This implies that low-frequency wave-quantity magnitudes using the invariant cross-sectional area only uniquely characterize the middle ear under the assumption that the middle-ear impedance $|Z_{me}| > Z_0$. However, temporal characteristics of reflectance may still reveal if this condition is not satisfied because the direction of rotation on the Riemann sphere around the axis spanning from -1 to 1 with increasing kl_{ec} changes.

Figure 8 also illustrates the importance of selecting an invariant ear-canal cross-sectional area that is representative of the population; if the invariant area is off from the population mean, projections of normalized impedance onto the Riemann sphere would tend to skew more in one direction, generally producing larger variations in reflectance magnitude for smaller kl_{ec}. Fortunately, judging from the data of Voss *et al.* (2025), the current assumption of 44.2 mm^2 for adult ears, used in existing clinical instruments and in the vast majority of the literature, appears to be a reasonable approximation for the average ear-canal area between the ear probe and the tympanic membrane for the population. For infant ears below 6 months age, some instruments utilize the smaller assumed area of 17.8 mm^2 (Keefe and Simmons, 2003), prompting an abrupt arbitrary change to absorbance values, normative data, and interpretation at the intersection between the age groups—not because of anatomical differences but because of the change in assumed area.[11] Some authors have attributed differences in absorbance from this age group to slightly older ears to developmental changes (Zhao *et al.*, 2025), even though these differences might as well stem from the difference in assumed cross-sectional area. However, for infants, matching the assumed area to the population might be less of a concern because of their generally smaller ear canals, meaning that kl_{ec} is generally smaller at the same frequency. Note that all our anatomical ears fall into the adult category (older than 6 months) in terms of the assumed cross-sectional area in existing instruments (Table I), and even the small ear canal 6207L produced reflectances similar to the remaining canals when using an invariant cross-sectional area [Fig. 6(b)]. Therefore, it might be preferable to simply use the adult cross-sectional area of 44.2 mm^2 for ears of all ages, thus removing the arbitrary category separation for normative WAI data at 6 months age.

D. Quantities characterizing hearing ability

Determining a suitable quantity for characterizing the middle ear depends on whether the goal is a unique characterization of middle-ear status or a characterization of the role of the middle ear in sound perception. Although wave quantities calculated from the estimated or acoustical area do characterize a physical phenomenon in the ear canal, our results suggest that this phenomenon plays a negligible role in the acoustic transduction mechanism in the ear canal and middle ear responsible for low-frequency hearing. It should be emphasized that our results only suggest what these wave quantities do not describe; they reveal nothing about the actual role of wave quantities in describing this transduction process and hearing at higher frequencies. However, as would be expected from a transmission line disregarding higher-order modes, our results do seem to imply that the relevancy of wave quantities in describing middle-ear mechanics is a gradual transition from no relevancy to sole relevancy in the hypothetical limits of zero and infinite frequency, respectively. The actual role of sound wave reflections and the relevance of wave quantities in characterizing the role of the middle ear in sound perception toward higher audio frequencies is not known, and no studies have investigated which quantities most accurately achieve this. However, it does seem plausible that wave quantities based on estimated or geometrical ear-canal cross-sectional areas, thus providing a characterization of the underlying physical wave phenomenon but a non-unique characterization of the middle ear, are the most relevant for this purpose. Still, although the cochlear immittance may affect the middle-ear immittance, the proportion of sound in the ear canal absorbed by the middle ear likely does not relate directly to that entering the cochlea because the middle ear includes several additional possible paths of transmission. A study investigating this might explore the relationship between air-bone gaps and various WAI quantities or follow the framework underlying Souza *et al.* (2014), mapping instead the relationship between changes in various WAI quantities and behavioral thresholds upon changes in middle-ear status, for example, induced by a static change in ear-canal air pressure. However, like Souza *et al.* (2014), the highly variable measurement uncertainty of individual WAI quantities needs to be taken into account in such studies. Regardless of the potential ability of wave quantities in characterizing hearing at higher frequencies, this does not change the fact that they do not provide a unique characterization of the middle ear, which might impact their ability to diagnose middle-ear pathologies.

The issues relating to the physical significance of wave quantities might, at least partly, explain the difficulty in their interpretation and relatively slow clinical adoption of WAI. Despite the results presented here, ear-canal wave quantities calculated using an invariant cross-sectional area does seem like a clinically viable measurement technique that can provide unique information on the middle-ear status up to approximately 3 kHz beyond what is possible with ear-canal immittance and conventional tympanometry. To improve our ability to uniquely characterize the middle ear across a wider frequency range, future research might preferably focus on methods to accurately and reliably measure or approximate the middle-ear immittance.

E. Reflectance-based stimulus quantities

Although wave quantities calculated from the estimated cross-sectional area might not be optimal for middle-ear diagnostics in the clinic, at least at low frequencies, because they are confounded by the canal area, they do provide improved accuracy for reflectance-based quantities for delivering stimuli to the ear (Souza *et al.*, 2014; Nørgaard and Bray, 2023) and measuring otoacoustic emissions (Charaziak and Shera, 2017). This is because these methods aim to describe the physical ear-canal sound field close to the tympanic membrane based on propagating waves rather than the mechanics of the middle ear, which is exactly what these wave quantities characterize. Evaluating the accuracy of stimulus levels and otoacoustic-emission measurements within our methodological framework could be achieved using a miniature microphone to measure stimulus levels and a speaker to simulate otoacoustic-emission responses, respectively, built into the middle-ear simulator at the plane of the middle ear, and constitutes a feasible extension of this study.

VI. CONCLUSION

This study has investigated the physical significance of ear-canal wave quantities, e.g., pressure reflectance and energy absorbance, and their variability due to variations in ear-canal geometry. This was done using a simple simulation approach based on lumped-element and transmission-line models, and 3D-printed uniform and anatomical ear canals terminated by the same middle-ear simulator. Our results showed the following:

(1) Ear-canal wave quantities characterize the wave interaction between the ear canal and middle ear, and do therefore not uniquely describe middle-ear mechanics. Variations in ear-canal geometry confound wave quantities calculated using the estimated or acoustical cross-sectional area, introducing significant inter-subject variability. In our anatomical ear canals, this estimated area based on Nørgaard *et al.* (2019c) appeared to approximate the longitudinally averaged area. On the other hand, middle-ear immittance quantities do uniquely characterize the middle ear, and although we were able to accurately estimate these quantities in ideal uniform ear canals, we were unable to do this in our anatomical ear canals using estimated uniform and known acoustical non-uniform ear-canal area functions.
(2) Among our considered quantities, wave quantities based on the assumption of an invariant cross-sectional area representative of the adult ears seem most suitable for clinical assessment of middle-ear status at frequencies below approximately 3 kHz because of their low sensitivity to variations in ear-canal geometry. These wave quantities do not provide a physical characterization of the middle ear at any frequency but may instead enable middle-ear diagnoses through pattern recognition. Deep ear-probe insertions may reduce measurement errors because of reflections at frequencies below the approximate 3-kHz limit. None of our considered quantities provided reliable unique characterizations of the middle ear in our anatomical ear canals above 3 kHz. Due to their smaller size, the same adult area might also be preferable in infant ears.
(3) Ear-canal wave quantities calculated using the estimated cross-sectional area do characterize an actual physical phenomenon at low frequencies. However, because the wavelength is much longer than the ear canal, the sound field is practically uniform, and effectively only a single impedance mismatch is present between a sound source and the ear canal. Therefore, the reflection of ear-canal sound waves by the middle ear plays a negligible role in the underlying acoustic transduction mechanism, which is instead dominated by the impedance mismatch directly between the sound source and the combined ear canal and middle ear. Therefore, ear-canal wave quantities do not provide a meaningful physical characterization of middle-ear mechanics at lower frequencies.

SUPPLEMENTARY MATERIAL

See the supplementary material for the measurement data in the uniform and anatomical ear canals presented in Secs. IV B and IV C; a MATLAB script to reproduce Figs. 2, 5, and 6; and a MATLAB script to produce the Riemann-sphere projections in Fig. 8. The scripts were tested in MATLAB R2025b, requiring no additional toolboxes. The measurement data may serve as a means for interested readers for evaluating their own or alternative algorithms for estimating the ear-canal cross-sectional areas, ear-canal area function, middle-ear immittance, etc. These data are made available for self-use only, and any publication of results based on the data is subject to approval by the authors of this article.

ACKNOWLEDGMENTS

This work was partly funded by the National Institutes of Health, Grant No. R15 DC014129-03A1 (S.E.V.).

AUTHOR DECLARATIONS

Conflict of Interest

K.M.N. is employed by Interacoustics A/S, a commercial company developing and manufacturing audiological instruments. Interacoustics A/S is involved and has an interest in promoting the commercialization of WAI. J.J.F. and S.E.V. have no conflicts to disclose.

DATA AVAILABILITY

The measurement data that support the findings of this paper are available in the supplementary material to this article. CT images were obtained retrospectively from the University of Massachusetts (UMass) Memorial Medical Center imaging archive. The institutional review board (IRB) at both the UMass Chan Medical School and Smith College granted exemptions from IRB oversight because of the de-identified nature of the material. We do not have permission to share physical aspects, such as the 3D-printed canals, from these scans.

[1]Based on other articles citing Hudde (1980), it appears that he introduced the concept of ear-canal energy reflectance in this PhD thesis prior to Stinson *et al*. (1982), but it was not possible to obtain a copy of the thesis online.

[2]Our approach is not possible using a standardized occluded-ear simulator (IEC 60318-4, 2010) because it includes a uniform portion of the ear canal that cannot be altered.

[3]Available at https://www.slicer.org (Last viewed 23 February 2026).

[4]The tympanic annulus and canal entrance planes were determined *via* coordinates obtained from the software OSIRIX and methods described by Balouch *et al*. (2023) and Voss *et al*. (2025).

[5]Available at https://github.com/wjakob/instant-meshes (Last viewed 23 February 2026).

[6]Specifically, *QUAD REMESHING* was performed within INSTANT MESHES, adjusting vertex count (1–5k) and smoothing iterations (0–4) as needed.

[7]See https://vtk.org/ (Last viewed 23 February 2026.).

[8]Available at https://github.com/KIT-IBT/vtkToolbox (Last viewed 23 February 2026).

[9]Available at playrec.co.uk (Last viewed 14 March 2025).

[10]mmho is conventionally used as the unit for admittance in tympanometry with $1\,\text{mmho} = 10^{-8}\text{m}^3/(\text{Pa}\cdot\text{s})$.

[11]Measurements of absorbance using the Titan (Interacoustics A/S, Middelfart, Denmark) were originally based on the calibration method described by Keefe and Simmons (2003) using two waveguides with the smaller area of $17.8\,\text{mm}^2$ for infants and two waveguides with a larger area of $49.5\,\text{mm}^2$ for adults. Their calibration method characterized the ear probe by its reflectance source parameters, meaning that the cross-sectional area of the calibration waveguides are encoded into the source parameters and implicitly assumed when calculating reflectance based on the two different sets of source parameters, infant and adult. This is in contrast to characterizing the ear probe based on its Thévenin-equivalent parameters, used here and in most of the research literature, which do not encode the cross-sectional area of the calibration waveguides (Nørgaard and Hajicek, 2022), and the assumption of cross-sectional area is not imposed until ear-canal reflectance is calculated, as in Eq. (3). Later, when a new calibration procedure based on Nørgaard *et al*. (2017b) was introduced into the Titan instrument, the adult area was changed to $44.2\,\text{mm}^2$ to align with competing instruments, but the smaller area for the age group below 6 months of age currently remains.

Al-Salim, S., Skretta, D., and Merchant, G. R. (**2024**). "Survey of wideband acoustic immittance use by clinical audiologists," Am. J. Audiol. **33**, 254–268.

Allen, J. B. (**1986**). "Measurement of eardrum acoustic impedance," in *Peripheral Auditory Mechanisms*, edited by J. Allen, J. Hall, A. Hubbard, S. Neely, and A. Tubis (Springer, Berlin), pp. 44–51.

Allen, J. B. (**2020**). *An Invitation to Mathematical Physics and Its History* (Springer, Cham, Switzerland).

Balouch, A. P., Bekhazi, K., Durkee, H. E., Farrar, R. M., Sok, M., Keefe, D. H., Remenschneider, A. K., Horton, N. J., and Voss, S. E. (**2023**). "Measurements of ear-canal geometry from high-resolution CT scans of human adult ears," Hear. Res. **434**, 108782.

Benade, A. H. (**1988**). "Equivalent circuits for conical waveguides," J. Acoust. Soc. Am. **83**, 1764–1769.

Caussé, R., Kergomard, J., and Lurton, X. (**1984**). "Input impedance of brass musical instruments—Comparison between experiment and numerical models," J. Acoust. Soc. Am. **75**, 241–254.

Charaziak, K. K., and Shera, C. A. (**2017**). "Compensating for ear-canal acoustics when measuring otoacoustic emissions," J. Acoust. Soc. Am. **141**, 515–531.

Feeney, M. P., Grant, I. L., and Marryott, L. P. (**2003**). "Wideband energy reflectance measurements in adults with middle-ear disorders," J. Speech Lang. Hear. Res. **46**, 901–911.

Feeney, M. P., Hunter, L. L., Kei, J., Lilly, D. J., Margolis, R. H., Nakajima, H. H., Neely, S. T., Prieve, B. A., Rosowski, J. J., Sanford, C. A., Schairer, K. S., Shahnaz, N., Stenfelt, S., and Voss, S. E. (**2013**). "Consensus statement: Eriksholm Workshop on Wideband Absorbance Measures of the Middle Ear," Ear Hear. **34**, 78S–79S.

Feng, J. J. (**2024**). "Effects of ear canal geometry on normative adult wideband acoustic immittance (WAI) measurements," Honors project, Smith College, Northampton, MA.

Huang, G. T., Rosowski, J. J., Puria, S., and Peake, W. T. (**2000**). "A noninvasive method for estimating acoustic admittance at the tympanic membrane," J. Acoust. Soc. Am. **108**, 1128–1146.

Hudde, H. (**1980**). "Messung der Trommelfellimpedanz des menschlichen Ohres bis 19 kHz," ("Measurement of the eardrum impedance of the human ear up to 19 kHz"), Ph.D. thesis, Ruhr-Universität Bochum, Bochum, Germany.

Hudde, H. (**1983**). "Measurement of the eardrum impedance of human ears," J. Acoust. Soc. Am. **73**, 242–247.

Hudde, H., and Schmidt, S. (**2009**). "Sound fields in generally shaped curved ear canals," J. Acoust. Soc. Am. **125**, 3146–3157.

IEC 60318-4 (**2010**). *Occluded-Ear Simulator for the Measurement of Earphones Coupled to the Ear by Means of Ear Inserts* (International Electrotechnical Commission, Geneva, Switzerland).

Keefe, D. H. (**1997**). "Otoreflectance of the cochlea and middle ear," J. Acoust. Soc. Am. **102**, 2849–2859.

Keefe, D. H. (**2020**). "Causality-constrained measurements of aural acoustic reflectance and reflection functions," J. Acoust. Soc. Am. **147**, 300–324.

Keefe, D. H., Folsom, R. C., Gorga, M. P., Vohr, B. R., Bulen, J. C., and Norton, S. J. (**2000**). "Identification of neonatal hearing impairment: Ear-canal measurements of acoustic admittance and reflectance in neonates," Ear Hear. **21**, 443–461.

Keefe, D. H., Hunter, L. L., Feeney, M. P., and Fitzpatrick, D. F. (**2015**). "Procedures for ambient-pressure and tympanometric tests of aural acoustic reflectance and admittance in human infants and adults," J. Acoust. Soc. Am. **138**, 3625–3653.

Keefe, D. H., Ling, R., and Bulen, J. C. (**1992**). "Method to measure acoustic impedance and reflection coefficient," J. Acoust. Soc. Am. **91**, 470–485.

Keefe, D. H., and Simmons, J. L. (**2003**). "Energy transmittance predicts conductive hearing loss in older children and adults," J. Acoust. Soc. Am. **114**, 3217–3238.

Lewis, J. D., and Neely, S. T. (**2015**). "Non-invasive estimation of middle-ear input impedance and efficiency," J. Acoust. Soc. Am. **138**, 977–993.

Merchant, G. R., and Neely, S. T. (**2021**). "The influence of otitis media with effusion on middle-ear impedance estimated from wideband acoustic immittance measurements," J. Acoust. Soc. Am. **150**, 969–978.

Møller, H. (**1992**). "Fundamentals of binaural technology," Appl. Acoust. **36**, 171–218.

Møller, H., Sørensen, M. F., Hammershøi, D., and Jensen, C. B. (**1995**). "Head-related transfer functions of human subjects," J. Audio Eng. Soc. **43**, 300–321.

Nørgaard, K. M. (**2023**). "A reference for ear-canal absorbance based on semi-anechoic waveguides," J. Acoust. Soc. Am. **154**, 2227–2235.

Nørgaard, K. M., and Bray, P. J. (**2023**). "Comments on forward pressure and other reflectance-based quantities for delivering stimuli to the ear," J. Acoust. Soc. Am. **153**, 909–920.

Nørgaard, K. M., Fernandez-Grande, E., Schmuck, C., and Laugesen, S. (**2020**). "Reproducing ear-canal reflectance using two measurement techniques in adult ears," J. Acoust. Soc. Am. **147**, 2334–2344.

Nørgaard, K. M., and Hajicek, J. J. (**2022**). "A systematic study on effects of calibration-waveguide geometry and least-squares formulation on ear-probe source calibrations," J. Acoust. Soc. Am. **151**, 634–649.

Nørgaard, K. M., Motallebzadeh, H., and Puria, S. (**2024**). "The influence of tympanic-membrane orientation on acoustic ear-canal quantities: A finite-element analysis," J. Acoust. Soc. Am. **155**, 2769–2785.

Nørgaard, K. R., Charaziak, K. K., and Shera, C. A. (**2019a**). "A comparison of ear-canal-reflectance measurement methods in an ear simulator," J. Acoust. Soc. Am. **146**, 1350–1361.

Nørgaard, K. R., Charaziak, K. K., and Shera, C. A. (**2019b**). "On the calculation of reflectance in non-uniform ear canals," J. Acoust. Soc. Am. **146**, 1464–1474.

Nørgaard, K. R., Fernandez-Grande, E., and Laugesen, S. (**2017a**). "Compensating for evanescent modes and estimating characteristic impedance in waveguide acoustic impedance measurements," J. Acoust. Soc. Am. **142**, 3497–3509.

Nørgaard, K. R., Fernandez-Grande, E., and Laugesen, S. (**2017b**). "Incorporating evanescent modes and flow losses into reference impedances in acoustic Thévenin calibration," J. Acoust. Soc. Am. **142**, 3013–3024.

Nørgaard, K. R., Fernandez-Grande, E., and Laugesen, S. (**2019c**). "Compensating for oblique ear-probe insertions in ear-canal reflectance measurements," J. Acoust. Soc. Am. **145**, 3499–3509.

Piskorski, P., Keefe, D. H., Simmons, J. L., and Gorga, M. P. (**1999**). "Prediction of conductive hearing loss based on acoustic ear-canal response using a multivariate clinical decision theory," J. Acoust. Soc. Am. **105**, 1749–1764.

Rabinowitz, W. M. (**1981**). "Measurement of the acoustic input immittance of the human ear," J. Acoust. Soc. Am. **70**, 1025–1035.

Rasetshwane, D. M., and Neely, S. T. (**2011**). "Inverse solution of ear-canal area function from reflectance," J. Acoust. Soc. Am. **130**, 3873–3881.

Souza, N. N., Dhar, S., Neely, S. T., and Siegel, J. H. (**2014**). "Comparison of nine methods to estimate ear-canal stimulus levels," J. Acoust. Soc. Am. **136**, 1768–1787.

Stinson, M. R., Shaw, E. A. G., and Lawton, B. W. (**1982**). "Estimation of acoustical energy reflectance at the eardrum from measurements of pressure distribution in the human ear canal," J. Acoust. Soc. Am. **72**, 766–773.

Voss, S. E., and Allen, J. B. (**1994**). "Measurement of acoustic impedance and reflectance in the human ear canal," J. Acoust. Soc. Am. **95**, 372–384.

Voss, S. E., Remenschneider, A. K., Farrar, R. M., Myoung, S., and Horton, N. J. (**2025**). "Comprehensive measurements and analyses of ear canal geometry from late infancy through late adulthood: Age-related variations and implications for basic science and audiological measurements," Trends Hear. (published online).

Xia, Y., Guo, Z., Tiana-Roig, E., Henriquez, V. C., and Lucklum, F. (**2024**). "Effect of curvature on sound propagation in the ear canal," J. Acoust. Soc. Am. **155**, 695–706.

Zhao, F., Suresh, S. C., Jones, E., Cao, Z., Zhang, L., Wang, J., Grais, E. M., Rajenderkumar, D., Lauxmann, M., and Jiang, W. (**2025**). "Age effect on wideband absorbance in people with normal middle ear function: A systematic review," Int. J. Audiol. (published online).